Packing of Ganglioside-Phospholipid Monolayers: An X-Ray Diffraction and Reflectivity Study

J. Majewski,* T. L. Kuhl,† K. Kjaer,‡ and G. S. Smith*

*Manuel Lujan Neutron Scattering Center, Los Alamos National Laboratory, Los Alamos, New Mexico 87545 USA; †Department of Chemical Engineering and Material Science, University of California, Davis, California 95616, USA; and ‡Department of Solid State Physics, Risø National Laboratory, DK-4000 Roskilde, Denmark

ABSTRACT Using synchrotron grazing-incidence x-ray diffraction (GIXD) and reflectivity, the in-plane and out-of-plane structure of mixed ganglioside-phospholipid monolayers was investigated at the air-water interface. Mixed monolayers of 0, 5, 10, 20, and 100 mol% ganglioside GM_1 and the phospholipid dipalmitoylphosphatidylethanolamine (DPPE) were studied in the solid phase at 23°C and a surface pressure of 45 mN/m. At these concentrations and conditions the two components do not phase-separate and no evidence for domain formation was observed. X-ray scattering measurements reveal that GM_1 is accommodated within the host DPPE monolayer and does not distort the hexagonal in-plane unit cell or out-of-plane two-dimensional (2-D) packing compared with a pure DPPE monolayer. The oligosaccharide headgroups were found to extend normally from the monolayer surface, and the incorporation of these glycolipids into DPPE monolayers did not affect hydrocarbon tail packing (fluidization or condensation of the hydrocarbon region). This is in contrast to previous investigations of lipopolymer-lipid mixtures, where the packing structure of phospholipid monolayers was greatly altered by the inclusion of lipids bearing hydrophilic polymer groups. Indeed, the lack of packing disruptions by the oligosaccharide groups indicates that protein-GM_1 interactions, including binding, insertion, chain fluidization, and domain formation (lipid rafts), can be studied in 2-D monolayers using scattering techniques.

INTRODUCTION

Lipid molecules containing sugar groups are called glycolipids. The most complex of these are the gangliosides, which contain one or more sialic acid residues and thus have a net negative change under physiological conditions. Glycolipids are present in most animal cell plasma membranes and are thought to play a role in a number of cellular functions, including cell recognition, adhesion, regulation, signal transduction, and development of tissues. They are predominantly located on the outer leaflet of the membrane and may act to protect the membrane from harsh conditions such as low pH or degradative enzymes (Alberts, 1994). Due to their charge, gangliosides also have significant effects on the electrical field across the membrane, and thus ion distribution (Beitinger et al., 1989). One of the more commonly studied gangliosides is galactosyl-*N*-acetylgalactosaminyl(*N*-acetyl-neuraminyl)galactosylglucosylceramide (GM_1). GM_1 is a member of the glycosphingolipids family and contains four neutral sugar residues and a negatively charged sialic acid residue (Fig. 1). A detailed description of the chemical, structural, and functional properties of GM_1 and glycolipids in general can be found in a review by Maggio (1994).

Recently, the formation of ganglioside (GM_1)-rich domains in monolayers and bilayers is an area of increased focus. In particular, specialized membrane domains composed of phospholipids, glycolipids, and cholesterol—so-called lipid rafts—are thought to play a role in a diverse range of processes ranging from membrane trafficking to signaling through specific membrane protein interactions where the raft microdomain acts as a platform for various cellular events (Simons and Ikonen, 1997). For example, high-resolution surface-sensitive techniques such as AFM have been used to probe the formation of submicrometer domains in phospholipid-GM_1 monolayers on solid supports (Yuan and Johnston, 2000; Vie et al., 1998). In these studies, GM_1 was heterogeneously distributed between liquid-expanded and condensed phases with clusters of GM_1-rich domains formed in the gel phase. However, the organization of GM_1-lipid mixtures is far from clear. For example, although electron spin resonance and freeze fracture studies have also implied clustering of GM_1 occurs in gel state lipids possibly due to carbohydrate-carbohydrate hydrogen-bonding interactions (Sharom and Grant, 1978; Peters et al., 1984; Delmelle et al., 1980), x-ray diffraction (McIntosh and Simon, 1994), differential scanning calorimetry (Bunow and Bunow, 1979; Sela and Bach, 1984), and freeze-etch electron microscopy measurements (Thompson et al., 1985) are consistent with a random distribution of the gangliosides in the various lipid structures investigated.

Here, we have focused on characterizing the structure of pure and mixed GM_1-phospholipid monolayers at the air-water interface using x-ray grazing-incidence diffraction and reflectivity measurements. We report detailed structural parameters for pure and mixed GM_1-phospholipid monolayers as a function of the ganglioside GM_1 concentration. These studies are the first in situ investigations of the structure of 2-D glycolipid-phospholipid monolayers at the

Received for publication 17 January 2001 and in final form 18 July 2001.

Address reprint requests to Dr. Tonya Kuhl, Dept. of Chemical Engineering and Material Science, University of California, Davis, CA 95616. Tel.: 530-754-5911; Fax: 530-752-1031; E-mail: tlkuhl@ucdavis.edu.

0006-3495/01/11/2707/09 $2.00

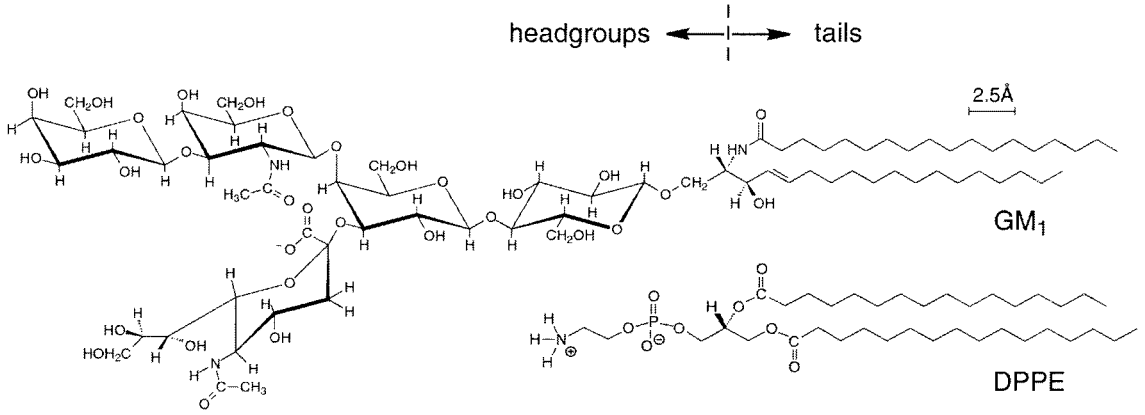

FIGURE 1 Chemical structure of DPPE and GM_1 molecules.

air-water interface. Our x-ray scattering data indicate that the glycolipid GM_1 is accommodated within the DPPE unit cell at least to concentrations of 20 mol % and that no lateral phase separation or lipid raft formation occurs.

EXPERIMENTAL METHODS

In general, Langmuir monolayers composed of 2-D crystallites, which are azimuthally randomly oriented on the water surface, may be described as 2-D powders. The reciprocal space GIXD patterns from 2-D ordered-crystalline monolayers on the liquid surface arise from a 2-D array of *Bragg rods*, which extend parallel to the vertical component, q_z, of the scattering vector, q (Als-Nielsen and Kjaer, 1989; Kjaer, 1994). To maximize surface sensitivity for GIXD measurements, the monochromatic x-ray beam was adjusted to strike the surface at an incident grazing angle 0.11°, 85% of the critical angle for total external reflection (Eisenberger and Marra, 1981). The dimensions of the footprint of the incoming x-ray beam on the liquid surface were $\sim 2 \times 50$ mm^2. For the collection of diffracted intensities we used a one-dimensional (1-D) position-sensitive detector (PSD) with its axis along the vertical and vertical acceptance $0 < q_z < 0.9$ Å^{-1}. In front of the PSD a Soller collimator was mounted, which defined the horizontal resolution of the detector, $\Delta q_{xy} = 0.0084$ Å^{-1}. The scattered intensity was measured by scanning over a range of the horizontal scattering vector component, $q_{xy} \approx (4\pi/\lambda)\sin(2\theta_{xy}/2)$, where $2\theta_{xy}$ is the angle between the incident and diffracted beam projected onto the horizontal plane, and λ is the wavelength of the x-ray beam. Such a scan, integrated over the whole window of the PSD, yields *Bragg peaks*. Simultaneously, the scattered intensity recorded in channels along the PSD, but integrated over the scattering vector in the horizontal plane across a Bragg peak, produces q_z-resolved scans called *Bragg rod profiles*. The intensity distribution along a Bragg rod can be analyzed by modeling the molecular conformation, packing, and orientation to yield, e.g., information on the direction and magnitude of the molecular tilt in the crystalline part of the amphiphilic film. In this work we modeled the lipid tails by a cylinder of constant electron distribution. Adjustable parameters, then, were the tilt angle of the cylinder from vertical, the lateral tilt direction, the length, L_c, of the cylinder (i.e., the length of the part of the molecule that scatters coherently), and the vertical root-mean-square displacement, σ_z (Debye-Waller factor), in the crystallites.

Detailed information on the electron density variation in the vertical direction, laterally averaged over both the ordered and disordered parts of the film, can be obtained from the deviation of the measured specular x-ray reflectivity from Fresnel's law (Als-Nielsen and Kjaer, 1989; Kjaer, 1994). The reflectivity data were analyzed using a kinematic approach (Als-Nielsen and Kjaer, 1989; Kjaer, 1994), assuming that the mixed monolayers formed homogeneous thin films. We used the simplest, physically reasonable model to fit the experimental data. A single Gaussian roughness was used to smear the interfaces and the resulting model reflectivity was compared to the data. The pure DPPE and GM_1 monolayers were modeled with two boxes; one for the headgroup and another for the hydrocarbon tail. For the mixed DPPE-GM_1 monolayers three boxes were necessary: one for the GM_1 headgroups and water, a second for the mixed DPPE and GM_1 headgroup region, and the third to describe the tail sections of both components.

By combining the methods of grazing-incidence x-ray diffraction and x-ray specular reflectivity, the in-plane and out-of-plane structure of these lipid films at air-liquid interfaces could be well-characterized. We performed the GIXD and reflectivity experiments at the BW1 (undulator) beam line at the HASYLAB synchrotron source (Hamburg, Germany) using a dedicated liquid surface diffractometer (Majewski et al., 1995; Weissbuch, et al., 1997). The amphiphilic monolayers were spread on a Millipore filtered water subphase from 5×10^{-7} molar 2:8 methanol-chloroform solutions. The trough was equipped with a Wilhelmy balance, a barrier for changing the surface area, and was thermostated to 23°C. After spreading a film, the trough container was flushed with helium gas to reduce the scattering background and to minimize beam damage during scans. As an additional precaution against beam damage the trough was translated by 0.025 mm, in the horizontal plane, perpendicular to the incoming beam at every step of the $2\theta_{xy}$ scan.

The pressure-area isotherms for the DPPE-GM_1 lipid mixtures are shown in Fig. 2. As can be seen, the lateral interactions due to the large oligosaccharide portion of the GM_1 headgroup result in a non-zero surface pressure even at areas per molecule above 100 Å^2 in the pure monolayer. In contrast, isotherms for the mixed DPPE-GM_1 up to 20 mol % can be almost superimposed on that of unmodified DPPE. In addition, no indication of domain formation, phase separation, or structuring within the monolayer at the air-water interface was observed using fluorescence or Brewster angle microscopy (results not shown). Homogeneous mixing of the two components is also indicated from the collapse pressures (Fig. 2). As shown, the collapse pressures of the mixtures fall in between those of pure DPPE and pure GM_1. Furthermore, the measured collapse pressure increased monotonically as the fraction of GM_1 in the mixture increased from 0 to 20 mol %. These data indicated that the mixtures behave ideally or nearly so in the experimentally relevant range of compositions. To investigate how the incorporation and size of the GM_1 headgroup affects the physical structure and packing within the monolayers (formation of lateral microdomains), GIXD and reflectivity measurements were conducted

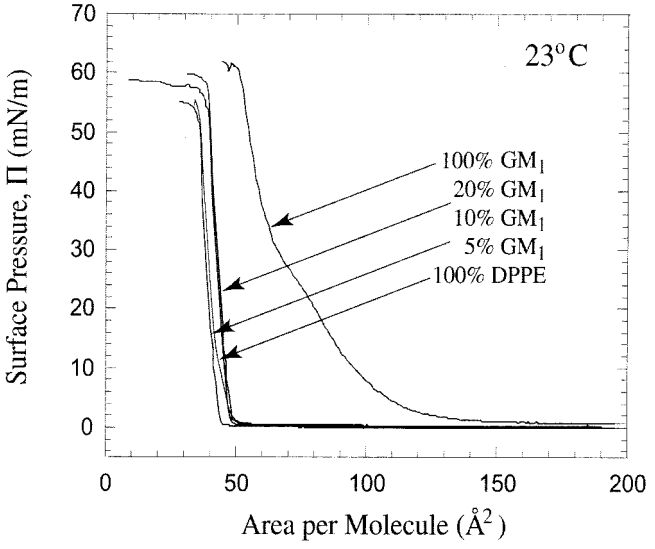

FIGURE 2 Monolayer compression (π-A) isotherms of pure DPPE, 95% DPPE-5% GM_1, 90% DPPE-10% GM_1, 80% DPPE-20% GM_1, and pure GM_1 at 23°C. The area, A, is the mean area per molecule at the air-water interface.

on pure GM_1 and DPPE monolayers and on three DPPE-GM_1 mixtures at a surface pressure of 45 mN/m.

RESULTS

Grazing-incidence x-ray diffraction

GIXD measurements provide structural information on the crystalline, diffracting portion of the monolayer. Diffraction data with both q_{xy} and q_z resolved (contour plot) for a pure GM_1 monolayer are shown in Fig. 3 *a*. Only one broad {1, 0} peak of low intensity was observed, which indicates hexagonal packing of the hydrocarbon tails with a unit cell dimension of $a_H = 4.87 \pm 0.01$ Å and low degree of in-plane crystallinity (small crystalline domain size). Fig. 3, *b* and *c* show the diffraction data projected on the q_{xy} and q_z axis, yielding Bragg peaks and Bragg rods, respectively. Analysis of the Bragg peak using the Scherrer formula (Guinier, 1968) gave an in-plane coherence length of a mere 50 ± 10 Å, indicative of small crystalline domains. The out-of-plane coherence length, L_c, obtained from fitting the Bragg rods was 19.0 ± 0.2 Å with negligible tilt. Structural parameters are summarized in Table 1. Interestingly, no diffraction signal was observed in the low q_{xy} region of the spectrum from the oligosaccharide headgroup of the GM_1 molecules.

Fig. 4 *a* shows the diffraction data (contour plots) for pure DPPE and mixed DPPE-GM_1 monolayers with both q_{xy} and q_z resolved. Fig. 4, *b* and *c* show the data projected on the q_{xy} and q_z axis, yielding Bragg peaks and Bragg rods, respectively. The structural parameters obtained from the fitting procedures for pure DPPE and the mixed DPPE-GM_1

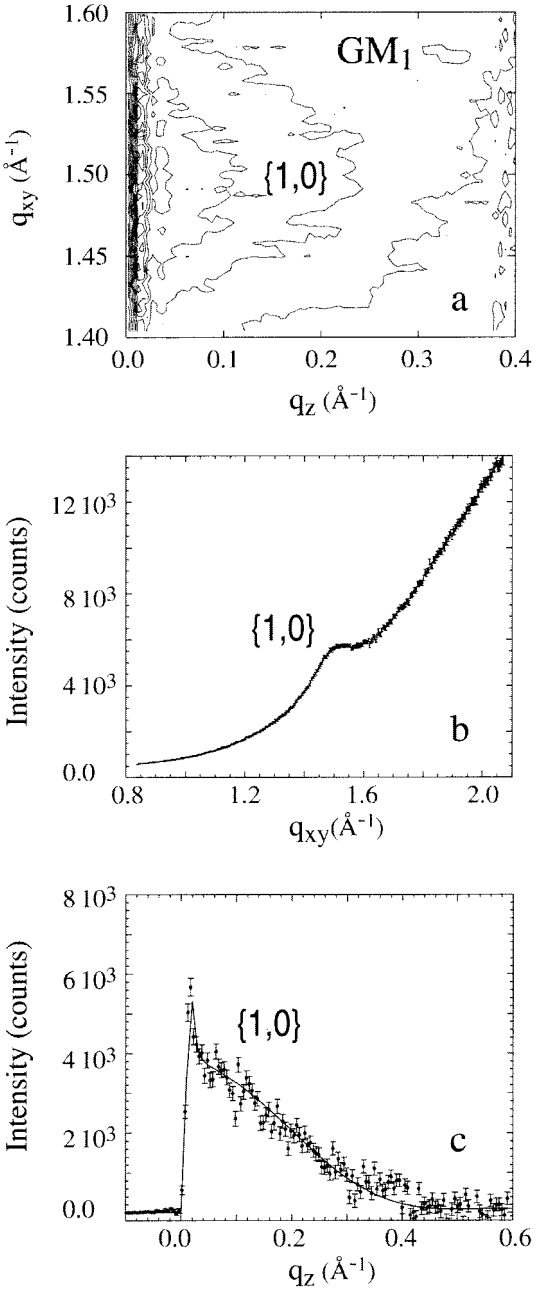

FIGURE 3 (*a*) The two-dimensional contour plots of the intensity distribution $I(q_{xy}, q_z)$ along the horizontal (q_{xy}) and the vertical (q_z) scattering vectors obtained for the pure GM_1 monolayer at a surface pressure of 45 mN/m and a temperature of 23°C. The single peak observed in (q_{xy}, q_z) space indicates a hexagonal unit cell. The maximum intensity along q_z at $\sim q_z = 0$ indicates little or no molecular tilt. (*b*) Grazing-incidence x-ray diffraction data. The Bragg peak profiles were obtained by scanning along the horizontal scattering vector q_{xy} ($q_{xy} \approx (4\pi/\lambda)\sin(2\theta_{xy}/2)$), where $2\theta_{xy}$ is the horizontal angle between the incident and diffracted beam and λ is the wavelength of the x-ray beam and integrating over the whole q_z window of the position sensitive detector. (*c*) Bragg rod-scattered intensity distribution perpendicular to the water surface and integrated (after background subtraction) over the q_{xy} range of the Bragg peak. The rod was fitted (*solid line*) by approximating the coherently scattering part of the GM_1 tail by a cylinder of a constant electron density. The molecular packing parameters used in the fitting procedure are listed in Table 1.

TABLE 1 GID parameters

Composition	Observed d-Spacing, Unit Cell (Å)*	In-Plane Bragg Peaks: Area per Molecule (Å^2)	In-Plane Bragg Peaks: Projected Area (Å^2)	In-Plane Bragg Peaks: Coherence Length, L (Å)	Out-of-Plane Bragg Rods: Coherence Length, L_c (Å)	Out-of-Plane Bragg Rods: Tilt Angle, t (°)	Out-of-Plane Bragg Rods: Tilt Direction (°)	Out-of-Plane Bragg Rods: σ_z (Å)‡
DPPE	$d_{\{1,0\}} = 4.16 \pm 0.01$ $a_H = 4.80 \pm 0.01$	39.9 ± 0.1	39.8 ± 0.1	$L_{10,01,1-1}$ 530 ± 10	18.8 ± 0.2	3.5 ± 0.5	n/a†	0.5
GM_1	$d_{\{1,0\}} = 4.22$ $a_H = 4.87$	41.1	40.9	$L_{10,01,\ 1-1}$ 50	19.0	6.0	n/a	0.5
95:5 DPPE/GM_1	$d_{\{1,0\}} = 4.17$ $a_H = 482$	40.2	40.1	$L_{10,01,\ 1-1}$ 530	18.8	3.5	n/a	0.5
90:10 DPPE/GM_1	$d_{\{1,0\}} = 4.17$ $a_H = 4.82$	40.2	40.1	$L_{10,01,\ 1-1}$ 525	18.8	3.5	n/a	0.5
80:20 DPPE/GM_1	$d_{\{1,0\}} = 4.17$ $a_H = 4.82$	40.2	40.1	$L_{10,01,\ 1-1}$ 520	18.8	3.5	n/a	0.5

*{hk} denotes a set of Bragg rods (hk) with equal in-plane components $|q_{xy}^{hk}|$, hence not resolved in GIXD from these 2-D powders, e.g., for a hexagonal lattice {10} means {(1 0), (0 1), ($\bar{1}$ 0), (0 $\bar{1}$), (1 $\bar{1}$), ($\bar{1}$ 1)}.

†The tilt direction is not well-determined for small tilt angle.

‡Because the intensity distribution in the Bragg rod is centered at small q_z, the measurements are insensitive to changes in σ_z.

monolayers are summarized in Table 1. For pure DPPE only one {1, 0} in-plane peak was observed, indicating the diffracting hydrocarbon chains have a hexagonal lattice, in agreement with previous results for diacyl phospholipid monolayers (Kjaer et al., 1987; Helm et al., 1987; Boehm et al., 1993). As shown in Fig. 4 *c*, the Bragg rods exhibit one broad maximum, located at $q_z \approx 0$ (Vineyard, 1982) [the sharp peak at $q_z = 0.01$ Å^{-1} is the so-called Vineyard-

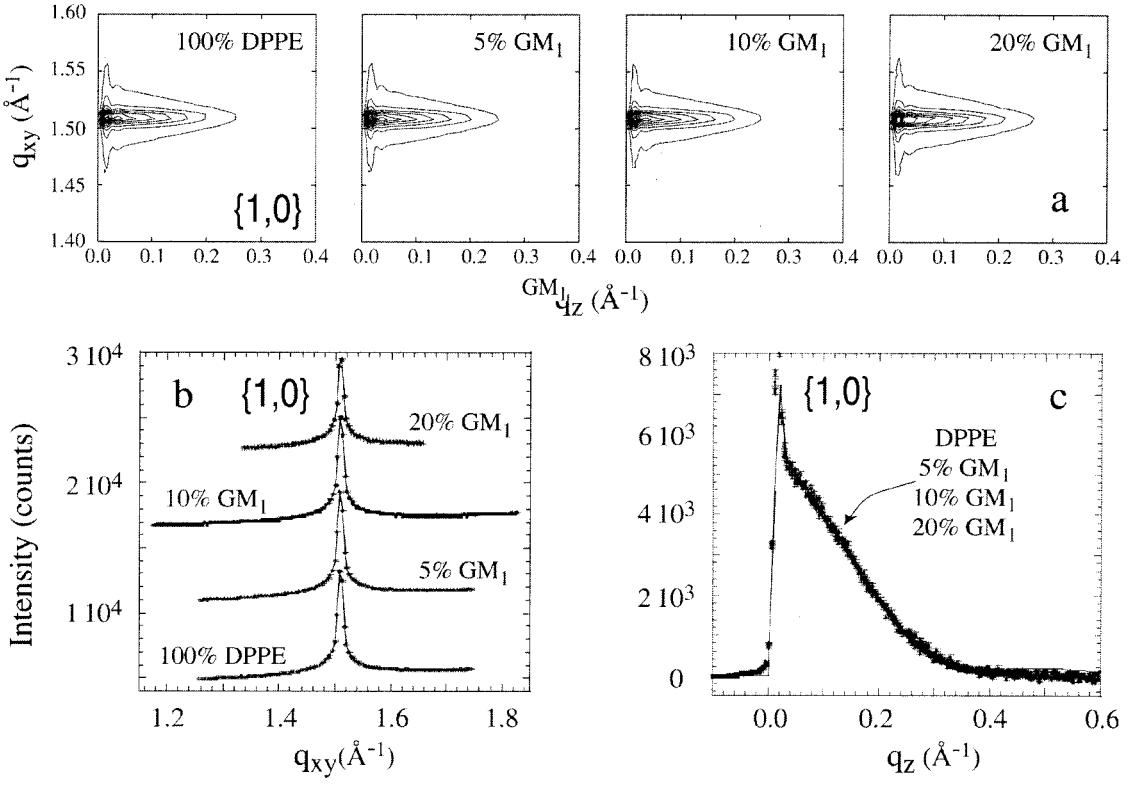

FIGURE 4 (*a*) The two-dimensional contour plots of the intensity distribution $I(q_{xy}, q_z)$ along the horizontal (q_{xy}) and the vertical (q_z) scattering vectors obtained for (*a*) *from left to right*: pure DPPE, 95% DPPE: 5% GM_1; 90% DPPE: 10% GM_1; 80% DPPE: 20% GM_1 monolayers at a surface pressure of 45 mN/m and 23°C. In all cases only one peak was observed in (q_{xy}, q_z) space indicating hexagonal unit cells. Along q_z the intensity has its maximum at $\sim q_z = 0$, indicating little or no molecular tilt. (*b*) Grazing-incidence x-ray diffraction measurements from pure DPPE and GM_1 mixtures. The Bragg peaks—as function of the horizontal scattering vector component, q_{xy}—were obtained from the data shown in (*a*) by integration over q_z. (*c*) Bragg rods—scattered intensity distribution perpendicular to the water surface and integrated (after background subtraction) over the q_{xy} range of each Bragg peak—for pure DPPE and GM_1 mixtures. The measured Bragg rods are identical. The rods were fitted (*solid lines*) by approximating the coherently scattering part of the monolayers by a cylinder of a constant electron density. The molecular packing parameters used in the fitting procedure are listed in Table 1.

Yoneda peak, which arises from the interference between x-rays diffracted up into the Bragg rod and rays diffracted down and then reflected up by the interface], indicating that the chains stand almost perpendicular to the air-water interface at high compressions of 45 mN/m. As evident from Fig. 4, mixing 5, 10, or 20 mol % GM_1 with DPPE does not induce any substantial change in the diffraction spectra: the lattice remains hexagonal, the q_{xy}-positions of Bragg peaks are the same for all the mixtures and very close to that of the pure DPPE, the integrated intensities and the shapes of the Bragg peaks are identical, and finally, the Bragg rods are superimposable.

Quantitatively, using the Scherrer formula (Guinier, 1968), the in-plane crystallite domain size is 525 ± 10 Å for pure DPPE and remains unchanged for the DPPE-GM_1 mixtures. The unit cell dimensions listed in Table 1 were obtained by fitting the peak positions, while the out-of-plane coherence lengths L_c were obtained by fitting the integrated Bragg rod intensities. The out-of-plane coherence length for a pure DPPE monolayer corresponds, as expected, to a fully stretched C_{15} chain, $L_c = 19.1$ Å (Als-Nielsen and Kjaer, 1989), again evidence that the tightly packed molecules stand almost perpendicular to the air-water interface. Surprisingly, the coherence length, L_c does not change significantly with the addition of GM_1, which suggests that the GM_1 molecules do not interfere with the packing of the hydrocarbon chains or protrude into solution, but rather are accommodated in the host, DPPE, monolayer. As a result, the unit cell and the packing of the molecules for the mixed monolayers are the same as pure DPPE.

Of particular importance in the GIXD data is the implied conclusion that no phase separation has occurred in the mixed GM_1-DPPE monolayers. Although neither Brewster angle nor fluorescent microscopy revealed domain formation, GIXD is extremely sensitive to the phase states of the lipid monolayers as described. First, there is no difference between the diffraction patterns or fitted parameters of pure DPPE or the various GM_1 mixtures. However, in these GIXD measurements only the crystalline portion of the hydrocarbon chains diffract the x-ray beam. Thus, one might suppose that some or all of the GM_1 is simply excluded from the crystalline DPPE monolayer, giving the same results as described above. For example, suppose that a portion of the monolayer was no longer diffracting, being in the amorphous state, upon the addition of GM_1. (An amorphous state must be assumed as no diffraction from a second crystalline phase is observed.) If one assumes that the added GM_1 is excluded from the host DPPE monolayer and stays in an amorphous state, the integrated intensity of the diffraction peak would decrease proportionally by the ratio of the areas occupied by the diffracting portions, a calculated decrease of 4, 9, and 18% as the concentration of GM_1 in the mixture increases to 20 mol %. The intensity drop is calculated assuming complete exclusion of GM_1 from the DPPE matrix, where the expected area per molecule for GM_1 is 65 $Å^2$ compared to 40 $Å^2$ for DPPE. However, we cannot preclude the possibility of a small portion of GM_1 being excluded from the mixed monolayer. Based on our measurements and associated errors, we estimate this as 2% (upper bound). Such decreases in intensity were not observed, providing strong evidence of miscibility in the DPPE-GM_1 mixtures. There is also no indication of phase separation in the size of the coherently scattering domains, which remain constant and equal to that of pure DPPE.

Reflectivity

In contrast to the GIXD measurements, x-ray reflectivity provides average structural information on both the 2-D-crystalline and amorphous parts of the monolayer. The reflectivity data were analyzed using the kinematical approach and the electron densities of the relevant chemical units were approximated with boxes of various thicknesses and electron densities (Als-Nielsen and Kjaer, 1989; Kjaer, 1994). The unmodified DPPE monolayer was modeled with two boxes (see Table 2, Fig. 5): one box for the headgroup region, 8.2 ± 0.2 Å long, with normalized electron density 1.49 ± 0.08 (all electron densities are reported normalized to that of the water subphase, $0.334e^-/Å^3$) and one box of length 18.8 ± 0.1 Å with electron density 0.988 ± 0.008 for the tail region, in agreement with previous studies of similar systems (Helm et al., 1987, 1991). During the refinement and model fitting the number of electrons in the tail region was fixed to values calculated from the chemical formula for DPPE and GM_1 to reduce the number of fitting parameters.

The reflectivity profile of the pure GM_1 monolayer could also be modeled with two boxes (see Table 2, Fig. 5): one extended box for the headgroup region, 18.6 ± 0.2 Å long with normalized electron density 1.56 ± 0.04, and one box of length 17.2 ± 0.1 Å and electron density 0.686 ± 0.005 for the tail region. The low electron density of the tail region corresponds to ~33 $Å^2$ per hydrocarbon chain on average, as expected from the isotherm (Fig. 2). Because reflectivity measurements average over the entire monolayer, the lower packing area of the hydrocarbon chains is detected. In contrast, in GIXD measurements only the crystalline hydrocarbon chains diffract, which have a correspondingly lower area per chain.

To obtain a good fit to the mixed DPPE-GM_1 reflectivity profiles two boxes were used to model the headgroup region, one box for the extended GM_1 headgroup and another for the mixed DPPE-GM_1 region. Parameters obtained from this fitting procedure are summarized in Table 2 and the fits are shown in Fig. 5. For the mixed monolayers, the tail region was 18.5 ± 0.3 Å thick and the electron densities of the tail region were constant, matching well to pure DPPE. This is another strong indication that phase separation of the two components does not occur, otherwise the average electron density of the tail region would be lower due to the

TABLE 2 Reflectivity parameters

Composition	Tail Region		DPPE/GM1 Headgroup Region		GM1 Head/Water Region				
	Thickness (Å)	Electron Density, ρ^* (#$e-$)	Thickness (Å)	Electron Density, ρ^* (#$e-$)	Thickness (Å)	Electron Density, ρ^* (#$e-$)	Area/mol. (Å^2)	σ (Å)	χ^2
DPPE	18.8 ± 0.1	0.988 ± 0.008 (242)†	8.2 ± 0.2	1.49 ± 0.08 (159) ± 7.5			39.0 ± 1.0	3.74 ± 0.05	43.0
GM_1	17.2	0.686 ± 0.005 (258)†	18.6 ± 0.2	1.56 ± 0.04 (633) ± 13			65.5 ± 1.5	4.85 ± 0.07	43.2
95:5 DPPE/GM_1	18.7	0.998 ± 0.002 (243)†	8.0 ± 0.4	1.51 ± 0.03 (157) ± 6	13.4 ± 1.0	1.08 ± 0.04 (188) ± 13	39†	3.72 ± 0.04	42.0
90:10 DPPE/GM_1	18.3	0.994 ± 0.001 (243)†	8.7 ± 0.4	1.45 ± 0.03 (169) ± 7	13.0 ± 0.5	1.13 ± 0.02 (197) ± 8	40†	3.64 ± 0.04	38.5
80:20 DPPE/GM_1	18.6	0.986 ± 0.002 (245)†	7.1 ± 0.6	1.47 ± 0.06 (139) ± 11	14.3 ± 0.5	1.24 ± 0.02 (236) ± 8	40†	3.71 ± 0.04	44.0

*All electron densities are normalized by the electron density of water, $\rho_{water} = 0.334e^-/Å^3$. σ is the r.m.s. roughness of the interface.
†Parameter fixed during refinement.

linear combination of the electron densities of the different domains/phases (high for DPPE and lower for GM_1 mixtures). Likewise, the thickness and electron densities of the mixed DPPE/GM_1 headgroup region obtained from the box model fitting did not change significantly, corresponding to the value obtained for pure DPPE. However, as stated above, an additional box was required to account for the extended GM_1 headgroup region. The electron density of this region increased approximately linearly with increasing concentration of the GM_1. The fitted value is slightly higher than that expected from a linear combination of electron densities of pure GM_1 and water, due to a more compact packing of GM_1 in the matrix of DPPE as compared to the pure GM_1 case. Comparing the number of electrons in the headgroup region obtained from fitting the reflectivity profile for the pure GM_1 monolayer with the expected number calculated from the chemical formula of the headgroup (579 electrons), suggests GM_1 headgroup structurally includes 5.5 water molecules on average. The hydration and ability of glycolipids to bind water has been previously well documented as observed here (Bach et al., 1982; Curatolo et al., 1977). Interestingly, the thickness of the GM_1 headgroup region was constant for all the mixtures and equal to 13.7 ± 0.7 Å. This thickness plus the length of the common GM_1/DPPE headgroup region (~8 Å) compares well to the expected size of the oligosaccharide headgroup of GM_1 of 21 Å reported previously (McIntosh and Simon, 1994). Thus, similar dimensions were obtained for the GM_1-phospholipid mixtures in 2-D monolayers as when incorporated into vesicular membranes.

DISCUSSION AND CONCLUSIONS

X-ray scattering data of DPPE-GM_1 mixed monolayers at the air-water interface have been presented. We studied pure DPPE, GM_1, and mixtures of 5, 10, and 20 mol % GM_1 matrixed with DPPE. No phase separation of components or lateral domain formation in these mixtures was detected. On the contrary, our GIXD and XR results indicate that in the series of DPPE-GM_1 mixtures investigated neither the in-plane nor out-of-plane packing of the monolayer changes relative to the host DPPE monolayer structure. The hexagonal unit cell dimensions, scattered intensity, and size of the crystallite domains of the composite monolayers remained unchanged. The out-of-plane coherently scattering portion of the lipid tails remained constant, matching closely that expected for a fully stretched C_{15} hydrocarbon chain, $L_c = 18.8 \pm 0.2$ Å. These GID measurements suggest that GM_1 glycolipids are accommodated within the DPPE unit cell for the concentrations studied, and that staggering of the DPPE or GM_1 lipids does not occur. Thus, there is no increase in the r.m.s. roughness of the monolayer as the GM_1 concentration increases. The packing arrangement can be visualized in the schematic (Fig. 6) where the DPPE headgroups and the proximal saccharide group of the GM_1 molecule line up in the 2-D monolayer

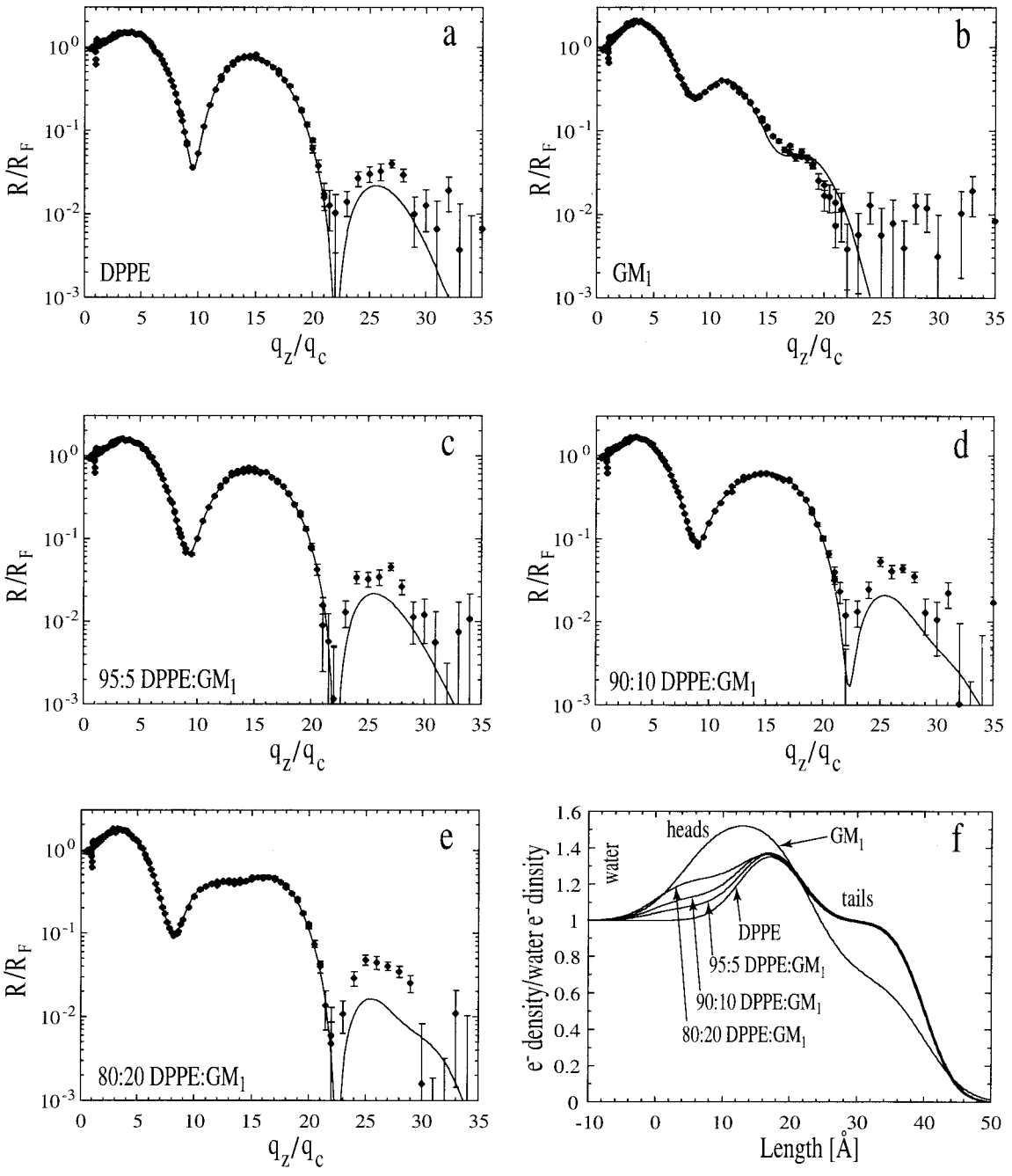

FIGURE 5 X-ray reflectivity data for (*a*) pure DPPE, (*b*) pure GM_1, (*c*) 95% DPPE: 5% GM_1, (*d*) 90% DPPE: 10% GM_1, (*e*) 80% DPPE: 20% GM_1 monolayers. The solid lines are fits to the data using box models discussed in the text. (*f*) The corresponding normalized electron density profiles obtained from the fitting parameters are listed in Table 2.

plane. The bulkier, branched portion of the oligosaccharide headgroup extends further into the water subphase, minimizing lateral interactions.

The oligosaccharide headgroup was easily detectable in the reflectivity profiles for the various compositions. The pure GM_1 monolayer was well-modeled with two boxes, one for the hydrocarbon tails and another for the extended headgroup region. The length of the boxes (17.2 + 18.6 Å, respectively) match well to the values obtained for a GM_1 molecule using an energy minimizing program [for visualizing the packing arrangements of the DPPE-GM_1 mixtures at the air-water interface and minimizing the energy of the single GM_1 and DPPE molecules to find their final conformations, we used the WebLab ViewerPro program by Molecular Simulations, Inc.]. However, the normalized electron density in the hydrocarbon tail region was significantly lower than that for a densely

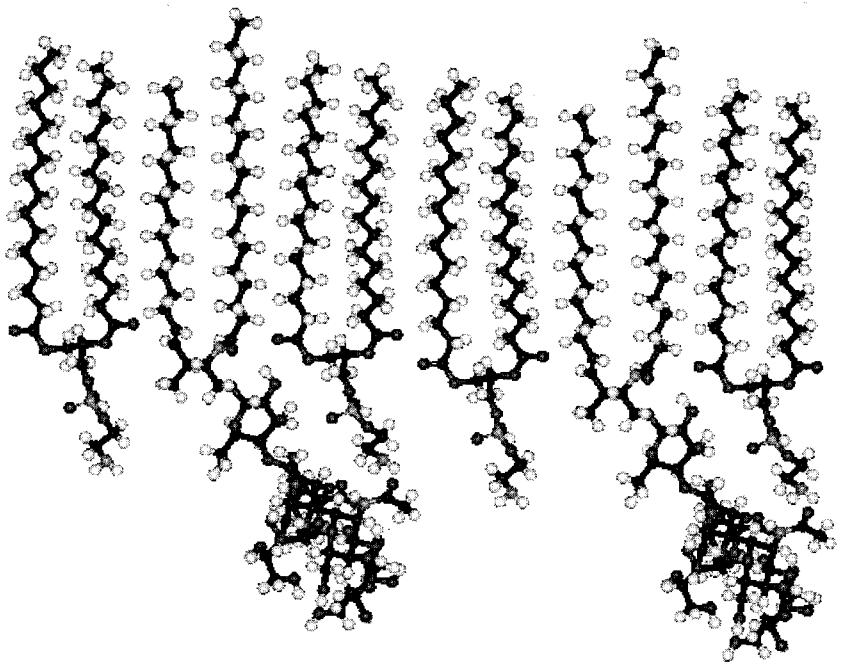

FIGURE 6 Schematic of the packing arrangement of DPPE-GM_1 mixtures at the air-water interface.

packed array, which indicates that the minimum packing area is limited by the lateral interactions between adjacent oligosaccharide headgroups in the pure glycolipid monolayer. These interactions result in an increase of area per molecule to 65.5 ± 1.5 Å^2, which is significantly larger than 40 Å^2 for two crystalline hydrocarbon chains.

With regard to the mixtures, the electron density of the GM_1 headgroup region increases proportionately with concentration. Based on the measured electron density, each oligosaccharide headgroup is well-hydrated and most likely structures/binds water. No evidence of oligosaccharide penetration into the hydrophobic regions of the lipid monolayer or staggering of the headgroups to reduce lateral headgroup-headgroup interactions was detected. Indeed, the electron density of the lipid tail region remains as that measured for a pure DPPE monolayer, which once again supports no phase separation of the components. These findings suggest that the monolayer packing of the mixtures is determined by the limiting area of the hydrocarbon tails, not the cross-sectional area of the oligosaccharide groups. From previous studies, the optimum headgroup area for a molecule of GM_1, as determined by light scattering measurements on ganglioside micelles, has been shown to be 95 Å^2 (Cantu et al., 1986). This presumably corresponds to the area at which the opposing forces of headgroup repulsion and interfacial attraction are balanced. Thus, at concentrations up to 20 mol %, where the area per oligosaccharide group is 200 Å^2, the influence of GM_1 glycolipids on DPPE monolayer dynamics and topology and presumably bilayers and membranes, in general, are likely not due to an effect on packing, but rather to the presence of the oligosaccharide groups at the monolayer surface as no evidence of phase separation, domain formation, or hydrocarbon chain fluidization was detected. However, it should be anticipated that lateral interactions between adjacent oligosaccharide headgroups will change packing in the hydrocarbon region at higher GM_1 concentrations. Based on our studies, new modes of packing should become important for GM_1-lipid proportions greater than 1:2 or ~30 mol %. These findings are supported by calorimetry measurements by Sillerud et al., 1979, who found that GM_1 could be substituted into a DPPC bilayer lattice at concentrations up to 25 mol %. However, studies in the literature have been contradictory regarding the formation of heterogeneous or homogeneous phases of lipid-glycolipid mixtures. For example, electron spin resonance and freeze fracture studies have implied clustering of GM_1 occurs in gel state lipids possibly due to carbohydrate-carbohydrate hydrogen bonding interactions (Sharom and Grant, 1978; Peters et al., 1984; Delmelle et al., 1980), while other studies indicate a random distribution of gangliosides in various lipid structures (Thompson et al., 1985; Bunow and Bunow, 1979; Sela and Bach, 1984). Interestingly, the matrix or host lipid in these earlier studies and most experimental work in general is phosphatidylcholine, whereas our studies have investigated the packing and incorporation of GM_1 into less hydrated phosphatidylethanolamine lipid monolayers (DPPE).

In summary, we have determined that GM_1 can be accommodated within the matrix of a host phosphatidylethanolamine lipid (DPPE) without altering the packing structure of the

monolayer at concentrations up to 20 mol %. This result does not support GM_1 clustering and suggests that 2-D monolayer studies utilizing scattering techniques may be ideal for probing the interaction of proteins, e.g., amyloid β peptide, cholera toxin, and myelin basic protein, with GM_1-bearing monolayers, as effects ranging from protein binding and insertion, fluidization, clustering, and domain formation could be followed quantitatively, which are active areas of investigation. (Choo-Smith and Surewicz, 1997; Terzi et al., 1997; Koppaka and Axelsen, 2000; Tomasi and Montecucco, 1981; Ong and Yu, 1984; Yanagisawa et al., 1995; Reed et al., 1987; Goins and Freire, 1985; Antes et al., 1992).

We thank Jacob Israelachvili for his help and advice and gratefully acknowledge beamtime at HASYLAB at DESY, Hamburg, Germany and funding by the programs DanSync (Denmark) and TMR-Contract ERBFMGECT950059 of the European Community.

This work was supported under the auspices of the United States Department of Energy and PECASE Award 05419-0099-2K, and the McCutchen Foundation. The Manuel Lujan Jr., Neutron Scattering Center is a national user facility funded by the United States Department of Energy, Office of Basic Energy Sciences-Materials Science, under contract W-7405-ENG-36 with the University of California.

REFERENCES

Alberts, B. 1994. Molecular Biology of the Cell, 3rd Ed. Garland Publishing Inc., New York.

Als-Nielsen, J., and K. Kjaer. 1989. X-ray reflectivity and diffraction studies of liquid surfaces and surfactant monolayers. *In* The Proceedings of the NATO Advanced Study Institute, Phase Transitions in Soft Condensed Matter; Geilo, Norway, April 4–14, 1989; Plenum Publishing Corp., New York. 113–137.

Antes, P., G. Schwarzmann, and K. Sandhoff. 1992. Detection of protein mediated glycosphingolipid clustering by the use of resonance energy transfer between fluorescent labeled lipids. A method established by applying the system ganglioside GM_1 and cholera toxin B subunit. *Chem. Phys. Lipids.* 62:269–280.

Bach, D., B. Sela, and I. R. Miller. 1982. Compositional aspects of lipid hydration. *Chem. Phys. Lipids.* 31:381–394.

Beitinger, H., V. Vogel, D. Mobius, and H. Rahmann. 1989. Surface potentials and electric dipole moments of ganglioside and phospholipid monolayers: contribution of the polar headgroup at the water/lipid interface. *Biochim. Biophys. Acta.* 984:293–300.

Boehm, C., H. Möhwald, L. Leiserowitz, J. Als-Nielsen, and K. Kjaer. 1993. Influence of chirality on the structure of phospholipid monolayers. *Biophys. J.* 64(2, Pt. 1):553–559.

Bunow, M. R., and B. Bunow. 1979. Phase behavior of ganglioside-lecithin mixtures. Relation to dispersion of gangliosides in membranes. *Biophys. J.* 27:325–337.

Cantu, L., M. Corti, S. Sonnino, and G. Tettamanti. 1986. Light scattering measurements on gangliosides: dependence of micellar properties on molecular structure and temperature. *Chem. Phys. Lipids.* 41:315–328.

Choo-Smith, L.-P., and W. K. Surewicz. 1997. The interaction between Alzheimer amyloid b(1-40) peptide and ganglioside G_{M1}-containing membranes. *FEBS Lett.* 402:95–98.

Curatolo, W., D. M. Small, and G. G. Shipley. 1977. Phase behavior and structural characteristics of hydrated bovine brain gangliosides. *Biochim. Biophys. Acta.* 468:11–20.

Delmelle, M., S. P. Dufrane, R. Brasseur, and J. M. Ruysschaert. 1980. Clustering of gangliosides in phospholipid bilayers. *FEBS Lett.* 121:11–14.

Eisenberger, P., and W. C. Marra. 1981. X-ray diffraction study of the Ge(001) reconstructed surface. *Phys. Rev. Lett.* 46:1081–1084.

Goins, B., and E. Freire. 1985. Lipid phase separations induced by the association of cholera toxin to phospholipid membranes containing ganglioside GM_1. *Biochemistry.* 24:1791–1807.

Guinier, A. 1968. X-ray Diffraction. Freeman, San Francisco.

Helm, C. A., H. Möhwald, J. Als-Nielsen, and K. Kjaer. 1987. Phospholipid monolayers between fluid and solid states. *Biophys. J.* 52:381–390.

Helm, C. A., P. Tippmann-Krayer, H. Möhwald, J. Als-Nielsen, and K. Kjaer. 1991. Phases of phosphatidyl ethanolamine monolayers studied by synchrotron x-ray scattering. *Biophys. J.* 60:1457–1476.

Kjaer, K. 1994. Some simple ideas on X-ray reflection and grazing-incidence diffraction from thin surfactant films. *Physica B.* 198:100–109.

Kjaer, K., J. Als-Nielsen, C. A. Helm, L. A. Laxhuber, and H. Möhwald. 1987. Ordering in lipid monolayers studied by synchrotron x-ray diffraction and fluorescence microscopy. *Phys. Rev. Lett.* 58:2224–2227.

Koppaka, V., and P. H. Axelsen. 2000. Accelerated accumulation of amyloid b proteins on oxidatively damaged lipid membranes. *Biochemistry.* 39: 10011–10016.

Maggio, B. 1994. The surface behavior of glycosphingolipids in biomembranes: a new frontier of molecular ecology. *Prog. Biophys. Mol. Biol.* 62:55–117.

Majewski, J., R. Popovitz-Biro, W. G. Bouwman, K. Kjaer, J. Als-Nielsen, M. Lahav, and L. Leiserowitz. 1995. The structural properties of uncompressed crystalline monolayers of alcohols $CH_{2n+1}OH$ (n = 13–31) on water and their role as ice nucleators. *Chemistry–A European Journal*. 1:304–312.

McIntosh, T. J., and S. A. Simon. 1994. Long- and short-range interactions between phospholipid/ganglioside GM1 bilayers. *Biochemistry.* 33: 10477–10486.

Ong, R. L., and R. K. Yu. 1984. Interaction of ganglioside GM_1 and myelin basic protein studied by carbon-13 and proton nuclear magnetic resonance spectroscopy. *J. Neurosci. Res.* 12:377–393.

Peters, M. W., I. E. Mehlhorn, K. R. Barber, and C. W. Grant. 1984. Evidence of a distribution difference between two gangliosides in bilayer membranes. *Biochim. Biophys. Acta.* 778:419–428.

Reed, R. A., J. Mattai, and G. G. Shipley. 1987. Interaction of cholera toxin with ganglioside GM_1 receptors in supported lipid monolayers. *Biochemistry.* 26:824–832.

Sela, B.-A., and D. Bach. 1984. Calorimetric studies on the interaction of gangliosides with phospholipids and myelin basic protein. *Biochim. Biophys. Acta.* 771:177–182.

Sharom, F. J., and C. W. M. Grant. 1978. A model for ganglioside behavior in cell membranes. *Biochim. Biophys. Acta.* 507:280–293.

Sillerud, L. O., D. E. Schafer, R. K. Yu, and W. H. Konigsberg. 1979. Calorimetric properties of mixtures of ganglioside GM_1 and dipalmitoylphosphatidylcholine. *J. Biol. Chem.* 254:10876–10880.

Simons, K., and E. Ikonen. 1997. Functional rafts in cell membranes. *Nature.* 387:569–572.

Terzi, E., G. Holzemann, and J. Seelig. 1997. Interaction of Alzheimer β-amyloid peptide(1–40) with lipid membranes. *Biochemistry.* 36:14845–14852.

Thompson, T. E., M. Allietta, R. E. Brown, M. L. Hohnson, and T. W. Tillack. 1985. Organization of ganglioside GM1 in phosphatidylcholine bilayers. *Biochim. Biophys. Acta.* 817:229–237.

Tomasi, M., and C. Montecucco. 1981. Lipid insertion of cholera toxin after binding to GM_1-containing liposomes. *J. Biol. Chem.* 256:11177–11181.

Vie, V., N. Van Mau, E. Lesniewska, J. P. Goudonnet, F. Heitz, and C. Le Grimellec. 1998. Distribution of ganglioside GM_1 between two-component, two-phase phosphatidylcholine monolayers. *Langmuir.* 14:4574–4583.

Vineyard, G. 1982. Grazing-incidence diffraction and the distorted-wave approximation for the study of surfaces. *Phys. Rev. B.* 26:4146–4157.

Weissbuch, I., R. Popovitz-Biro, M. Lahav, L. Leiserowitz, K. Kjaer, and J. Als-Nielsen. 1997. Molecular self-assembly into crystals at air-liquid interfaces. *Adv. Chem. Phys.* 102:39–120.

Yanagisawa, K., A. Odaka, N. Suzuki, and Y. Ihara. 1995. GM_1 ganglioside-bound amyloid beta-protein (A beta): a possible form of preamyloid in Alzheimer's disease. *Nature Medicine.* 1:1062–1066.

Yuan, C., and L. J. Johnston. 2000. Distribution of ganglioside GM_1 in L-α-dipalmitoylphosphatidylcholine/cholesterol monolayers: a model for lipid rafts. *Biophys. J.* 79:2768–2781.